

Application of topological edge states in magnetic resonance imaging

Viktor M. Puchnin,¹ Olga V. Matvievskaya,¹ Alexey P. Slobozhanyuk,¹ Alena V. Shchelokova,^{1,*} and Nikita A. Olekhno^{1,*}

¹*School of Physics and Engineering, ITMO University, Saint Petersburg 197101, Russian Federation*

(Dated: October 19, 2022)

Topological edge states in electromagnetic systems feature a set of attracting fundamental properties and unveil prospective applications based on disorder robustness and tailored localization. Despite active efforts in implementing topologically-protected waveguides in 2D photonic systems, applications of 1D topological systems remain almost uncharted. This letter demonstrates that topological edge modes can be realized in metamaterial-inspired volumetric resonators with a practical application in clinical magnetic resonance imaging (MRI). Performing numerical simulations and experiments with a 1.5 T MR scanner, we reconstruct the associated topological edge mode profiles and demonstrate their feasibility for sensitivity enhancement of conventional radiofrequency coils.

Topological photonics addresses edge- and corner-localized excitations whose existence is governed by general symmetries of a supporting structure rather than by any specific modifications of its boundary [1]. Such symmetry protection leads to intriguing fundamental properties, including bulk-boundary correspondence, and induces increased robustness of topological edge states towards various imperfections in the host structure [2]. There are numerous realizations of topologically-protected edge states in electromagnetic systems ranging from classical [3–5] and quantum [6, 7] optics to gigahertz setups [8–10] with possible applications in signal multiplexers [11] and even low-frequency electrical circuits [12–16].

While the majority of the photonic topological insulators are designed to control edge [17] and surface [18] states, the abilities of 1D topological structures [19] to sculpt electromagnetic near fields in real-life applications remain limited and are represented mostly by wireless power transfer [20, 21] and analog signal processing [22, 23]. Assessing the potential of topological edge states in 1D structures to strongly localize and manipulate the field at the subwavelength scale can make them an essential platform for practical applications, for example, to improve magnetic resonance imaging (MRI) characteristics through local enhancement of the transmit efficiency as well as the increase in the sensitivity of the radiofrequency (RF) coils [24]. In particular, it was shown that a metamaterial-based resonator could be used for the realization of a wireless coil for breast MRI [25, 26]. However, the previously demonstrated design has limitations with required near-field profiles preventing full coverage of fibroglandular tissue, which may lead to limitations for a very comprehensive assessment.

In the present Letter, we demonstrate that topological edge states can be effectively implemented in a metamaterial-inspired volumetric resonator (dubbed

metasolenoid) [27] and used to overcome previous challenges in the resonator’s design for MRI (Fig. 1). Such a device inductively couples with a quadrature RF whole-body birdcage coil of an MR scanner and focuses its magnetic flux in a desired small region, maximizing the transmit efficiency and receive sensitivity of the body coil. Inducing a geometrical dimerization in such arrays of strongly coupled split-ring resonators (SRRs), we implement Su-Schrieffer-Heeger (SSH) model [28] and demonstrate that the topological edge mode emerges even in the presence of electromagnetic coupling between the considered metasolenoid and a body coil which excites circularly polarized RF magnetic field (B_1^+) in 1.5 T MR scanners. Moreover, the topological resonator itself does

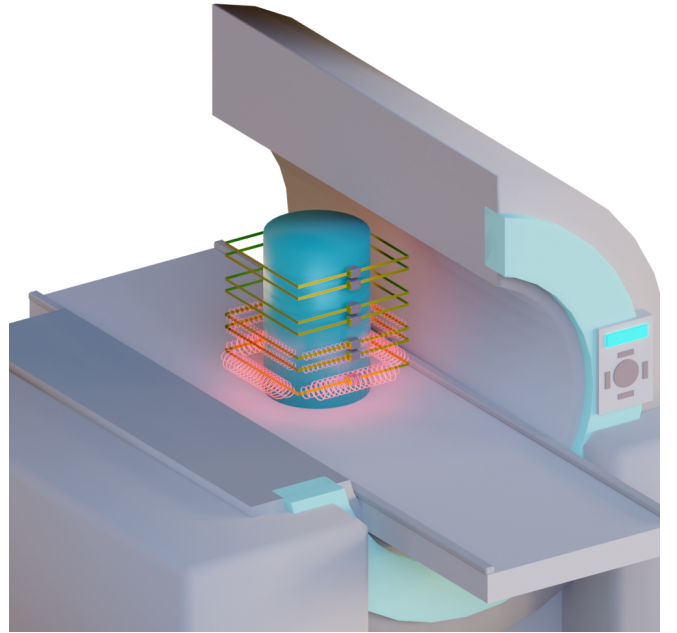


FIG. 1. Schematic view of a metamaterial-inspired volumetric resonator supporting a topological edge state (shown in red) together with a breast phantom (shown in teal color) located inside an MR scanner.

* These authors contributed equally to this work
Corresponding author: a.schelokova@metalab.ifmo.ru

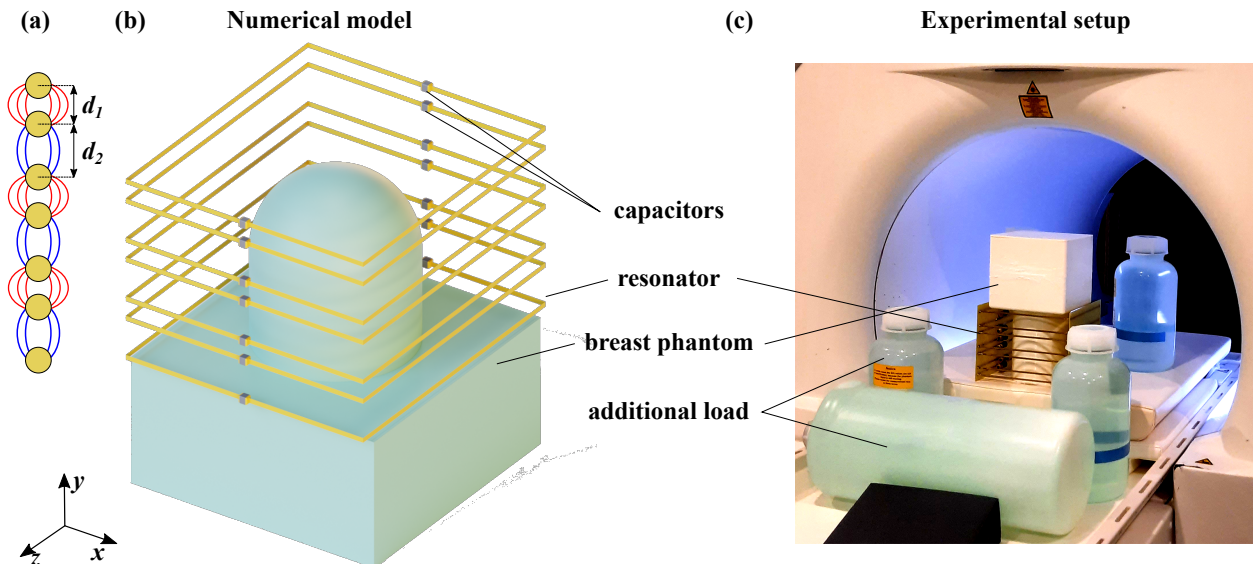


FIG. 2. (a) Schematic view of the 1D Su-Schrieffer-Heeger model with elements placed at alternating distances d_1 and d_2 . (b) Numerical model of the topological metasolenoid (yellow wires with capacitors) including a breast phantom (teal color). (c) Photograph of the experimental setup, featuring topological metasolenoid, the breast phantom, and additional load placed on the MR scanner table (different size bottles placed around the breast phantom).

not affect the polarization and magnitude of the RF magnetic field in the outer regions (i.e., does not disturb the functionality of the MR scanner), which allows probing such states with standard imaging pulse sequences and unveils prospects for their use in MRI. Finally, we estimate the signal-to-noise ratio (SNR) to demonstrate the efficiency and safety of the proposed topological metasolenoid.

We start with considering a plain (topologically trivial) metasolenoid similar to those studied in Refs. [26, 29], which consists of 7 SRRs that are placed periodically with $d = 18.5$ mm spacing forming an array with the height of 114 mm. Each split-ring resonator is formed by a rectangular copper frame with dimensions of 156×175 mm² and two gaps at the centers of the opposite sides. Then, a variable capacitor with a capacitance in the range 1 – 20 pF is placed in each gap to adjust the resonator’s resonance frequency to the Larmor frequency of the MR scanner. As demonstrated in Refs. [26, 29], such a resonator supports a highly homogeneous magnetic field in its volume, reaching a maximal amplitude at its center (see the supplementary material Figure S1 for details).

However, focusing RF fields at the metasolenoid edge (or even outside of it), as demonstrated in Fig. 1, might also be of interest for various applications (e.g., studying body region in the chest wall). While the standard metasolenoid design with evenly spaced SRRs clearly resembles Hubbard model [30] with eigenmodes delocalized over the bulk, its dimerized analog with alternating distances d_1 and d_2 should implement the celebrated SSH model [28] [Fig. 2(a)]. Such a model, in turn, demonstrates the presence of a spectral bandgap hosting an in-gap state localized at the edge and topologically pro-

ected by the chiral symmetry [2].

Introducing a dimerization, we consider the metasolenoid with $n = 7$ SRRs and the height of 114 mm, keeping spatial dimensions of the structure the same as in Ref. [26], Fig. 2(b,c). The distances between the nearest SRRs are $d_1 = 12.3$ mm and $d_2 = 24.7$ mm, respectively. In this case, the edge with the weak coupling d_2 features the presence of the topological edge state, in contrast to the edge with the strong coupling d_1 [2]. As shown in Fig. 2(b), we consider the geometry with the weak coupling located at the breast-body transition to concentrate the fields under the breast.

Numerical simulations of the topological metasolenoid were performed in CST Studio Suite 2021 using the eigenmode and time domain solvers. A volumetric resonator was loaded with a homogeneous phantom simulating the properties and dimensions of the breast and the part of the body with the following properties: the size of the body area is $160 \times 160 \times 80$ mm³, the dielectric constant of the body is $\epsilon = 78$, the conductivity is $\sigma = 0.45$ S/m; breast phantom parameters: the radius is 4.7 cm, the height is 10.34 cm, the dielectric constant is $\epsilon = 70$, and the conductivity is $\sigma = 0.2$ S/m.

The standard metasolenoid has several eigenmodes (see the supplementary material Figure S1), which differ in current and electromagnetic field distributions [31]. In addition, the uniform placement of SRRs is characterized by a symmetrical pattern of field distributions. The introduced dimerization qualitatively changes only the distribution of the fourth mode: the magnetic field concentrates near the edge SRRs, and in the rest of the resonator, the respective mode has an extremely low amplitude [Fig. 3(a)] characteristic of the SSH chain.

Most clinical MR scanners use an RF birdcage body coil to excite the MR signal, creating a rotating transverse RF magnetic field within its volume (see the supplementary material Figure S2). As a part of the numerical simulation, we used an emulator consisting of four pairwise orthogonal waveguide ports that allow us to create a similar circularly-polarized magnetic field. Each port was given a phase delay of 90° from the previous one to create a rotating magnetic field. The modified resonator loaded by a homogeneous phantom was placed at the center between all the ports. At the same time, the fourth resonant mode was tuned to 63.68 MHz by selecting the proper capacitance of variable capacitors. Thus, we demonstrate that the topologically protected edge mode of the SSH model can be excited in a rotating RF magnetic field. Due to the inductive coupling of the topological metasolenoid with the exciting ports, the magnetic flux is focused inside the area of interest, i.e. outside the internal volume of the resonator, Fig. 3(a). In addition, the maximum is located at a distance of 60 mm from the edge SRR.

The experimental prototype of the topological metasolenoid includes two arrays of 14×2 copper strips (each with sizes $75 \times 3 \text{ mm}^2$) printed on two dielectric FR4 substrates with sizes of $164 \times 114 \times 1 \text{ mm}^3$ characterized by the permittivity $\varepsilon = 4.3$ and losses $\tan \delta = 0.003$ at the frequency of 63.68 MHz. Each pair of copper strips on the same printed circuit board (PCB) is connected by variable capacitors with $C = 4 - 20 \text{ pF}$. The distances between pairs of SRRs are the same as used in numerical studies ($d_1 = 12.3 \text{ mm}$ and $d_2 = 24.7 \text{ mm}$). Two PCBs are connected using telescopic brass tubes. The breast phantom shell is 3D-printed using polylactic acid plastic (PLA) and has a height of 100 mm and a base radius of 50 mm. The phantom solution consists of distilled water, NaCl (0.75 g/l), agarose (10 g/l), and a gadolinium-based MRI contrast agent (0.5 ml/l) to reduce spin-lattice relaxation time T_1 . The phantom permittivity and conductivity were measured to be $\varepsilon = 78$ and $\sigma = 0.19 \text{ S/m}$ at 63.68 MHz using a coaxial probe (DAK-12, SPEAG, Zurich, Switzerland).

For tuning the fourth mode to the Larmor frequency, we measured the reflection spectra of the topological metasolenoid using a non-resonant loop antenna connected with a vector network analyzer Planar (s5048, Chelyabinsk, Russian Federation). The loop antenna was placed at the center of the edge SRR. The fourth peak on the spectrum corresponds to a topologically protected resonant mode (see the supplementary material Figure S3).

MRI experiments were performed on a 1.5 T clinical MR scanner (Siemens MAGNETOM Espree) at Federal Almazov North-West Medical Research Centre (Saint Petersburg, Russian Federation). The breast phantom was used as the object of the study, the experimental setup is demonstrated in Fig. 2(c). We also used a standard set of calibration body phantoms (Siemens) for additional load. The topological metasolenoid was placed on the patient

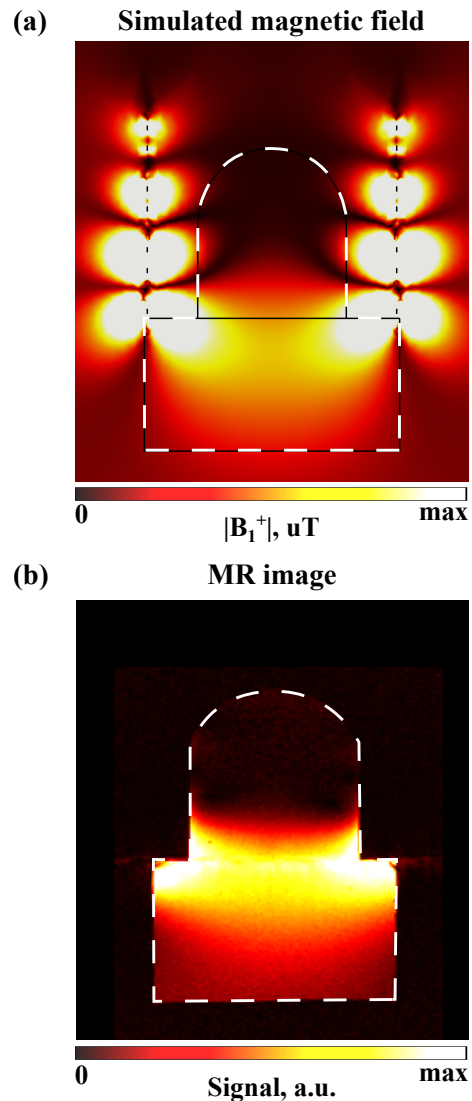


FIG. 3. (a) Numerical simulation results of the edge-localized mode showing the amplitude of RF magnetic field B_1^+ at the frequency $f = 63.68 \text{ MHz}$. The topological resonator is excited by the circularly polarized magnetic field induced by the four waveguide ports. (b) Experimentally obtained MR image of the breast phantom.

table with several foam pads for its positioning at the center of the MR scanner bore. The axis of symmetry of the resonator was in the plane of rotation of the transverse RF magnetic field of the whole-body coil embedded into the scanner bore. MR scanner's reference voltage (U_{ref}) was calibrated to ensure that the actual flip angle in the region of interest (ROI) was equal to 180 degrees. MR images of the breast phantom were obtained at the axial plane using a T_1 -weighted gradient echo sequence with the following parameters: echo time (TE)=4.76 ms, repetition time (TR)=2500 ms, flip angle= 20° , Field-Of-View= $260 \times 320 \text{ mm}^2$, matrix= 256×208 . The resulting MR image is shown in Fig. 3(b). The signal distribution on the image has the same behavior as in the nu-

merical results: it localizes between the breast and body parts, demonstrating an excitation of the topologically protected edge state in an SSH array of SRRs using a clinical 1.5 T MR scanner.

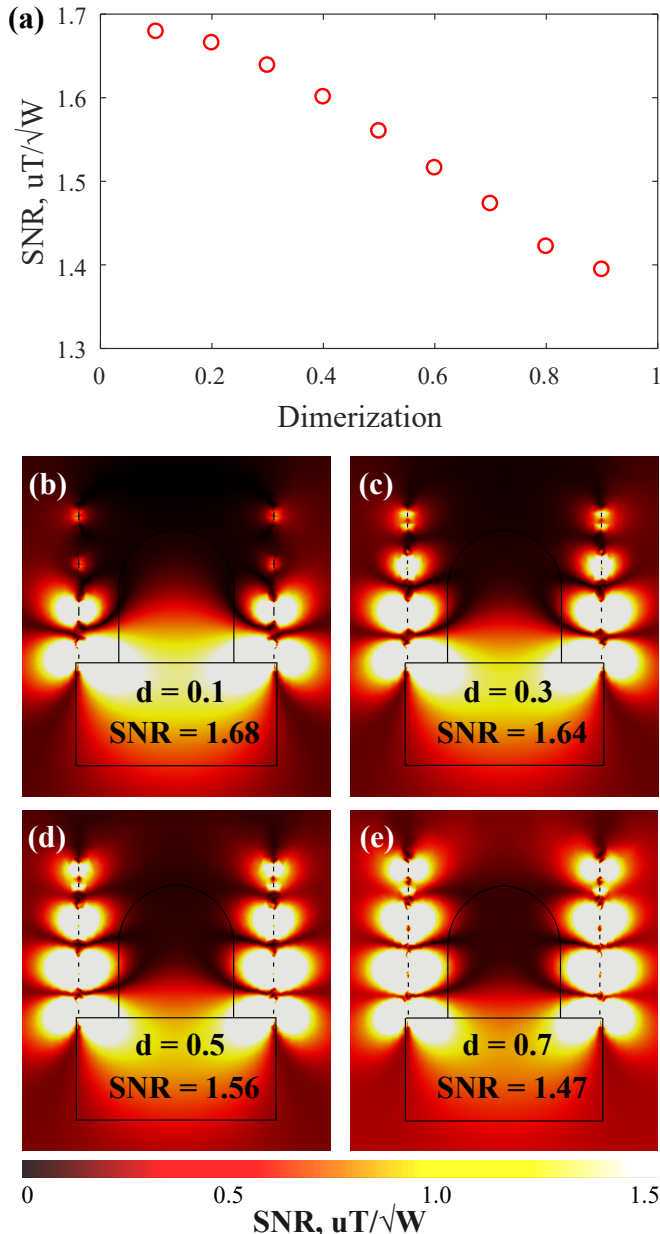


FIG. 4. (a) Signal-to-noise ratio (SNR) dependence on the dimerization degree. (b) Numerical model of the topological metasolenoid (yellow wires with capacitors), including a breast phantom. (b-e) SNR distributions for different dimerization degrees d : (b) $d = 0.1$, (c) $d = 0.3$, (d) $d = 0.5$, and (e) $d = 0.7$.

In the next stage, we consider numerically the ways to increase the efficiency of the proposed structure in terms of the SNR in the body region. In high-field MRI

systems, noise is proportional to the square root of the absorbed power, and the useful signal is proportional to the magnetic field. Therefore, in the first approximation, the SNR can be estimated as the ratio of the average value of the amplitude of the RF magnetic field to the square root of the power absorbed in the phantom. Figure 4(a) presents the SNR dependence on dimerization. Different configurations were considered by changing the distances between SRRs as a ratio d_1/d_2 where d_1 is the distance inside SRRs pairs and d_2 is the distance between SRRs pairs. The mean value of SNR was calculated in the body part of the phantom. The mean SNR reduces inside the phantom body with a further increase in the homogeneity of SRR's structure.

Figure 4(b)-(e) demonstrates SNR maps in the central slice of the phantom for four different values of dimerization. It is seen that for higher contrast between d_1 and d_2 , the SNR in the body phantom (imitating the chest wall area) becomes higher as well, facilitating an increase in the SNR for topological metasolenoid compared to the trivial one. These results are also supported by the measurements of the dependence of magnetic field amplitude on dimerization, showing an increase in the focusing of the magnetic field at the edge ring for higher contrasts between d_1 and d_2 (see the supplementary material Figure S4).

In this letter, we introduce a metamaterial-inspired resonator for MRI supporting a topologically protected edge mode and described by the 1D SSH model. Numerical simulations and experimental studies with a phantom reveal a strong localization of the RF magnetic field inside the body region under the breast, which is of key interest for searching breast cancer metastases [32]. We reveal an increase in SNR in the chest wall area for topological metasolenoid compared with the trivial one.

Prospective directions of further development include testing other quasi-one-dimensional topological models, including zig-zag arrays of SRRs [5, 33, 34], engineering the effects of long-range couplings [10, 35, 36], and considering non-linear effects in 1D SSH model [37] to open further degrees of tunability. Assessing the implementation of \mathcal{PT} -symmetric 1D SSH model with additional gain in SRRs [38] and topological metasolenoids with external optical switching [34] also looks very perspective.

ACKNOWLEDGMENTS

The authors acknowledge valuable discussions with Dr. Dmitry Zhirihin. A.P.S. acknowledges the support from the Foundation for Advancement of Theoretical Physics and Mathematics “BASIS.” The work was supported by the Ministry of Science and Higher Education of the Russian Federation (project No. 075-15-2021-1391).

- [1] Ling Lu, John D. Joannopoulos, and Marin Soljačić, “Topological photonics,” *Nature Photonics* **8**, 821–829 (2014).
- [2] Tomoki Ozawa, Hannah M. Price, Alberto Amo, Nathan Goldman, Mohammad Hafezi, Ling Lu, Mikael C. Rechtsman, David Schuster, Jonathan Simon, Oded Zilberberg, and Iacopo Carusotto, “Topological photonics,” *Reviews of Modern Physics* **91**, 015006 (2019).
- [3] M. Hafezi, S. Mittal, J. Fan, A. Migdall, and J. M. Taylor, “Imaging topological edge states in silicon photonics,” *Nature Photonics* **7**, 1001–1005 (2013).
- [4] Babak Bahari, Abdoulaye Ndao, Felipe Vallini, Abdelkrim El Amili, Yeshiahu Fainman, and Boubacar Kanté, “Nonreciprocal lasing in topological cavities of arbitrary geometries,” *Science* **358**, 636–640 (2017).
- [5] Sergey Kruk, Alexander Poddubny, Daria Smirnova, Lei Wang, Alexey Slobozhanyuk, Alexander Shorokhov, Ivan Kravchenko, Barry Luther-Davies, and Yuri Kivshar, “Nonlinear light generation in topological nanostructures,” *Nature Nanotechnology* **14**, 126–130 (2019).
- [6] Andrea Blanco-Redondo, Bryn Bell, Dikla Oren, Benjamin J. Eggleton, and Mordechai Segev, “Topological protection of biphoton states,” *Science* **362**, 568–571 (2018).
- [7] Sunil Mittal, Elizabeth A. Goldschmidt, and Mohammad Hafezi, “A topological source of quantum light,” *Nature* **561**, 502–506 (2018).
- [8] Christopher W. Peterson, Wladimir A. Benalcazar, Taylor L. Hughes, and Gaurav Bahl, “A quantized microwave quadrupole insulator with topologically protected corner states,” *Nature* **555**, 346–350 (2018).
- [9] Yuan Li, Yong Sun, Weiwei Zhu, Zhiwei Guo, Jun Jiang, Toshikaze Kariyado, Hong Chen, and Xiao Hu, “Topological LC-circuits based on microstrips and observation of electromagnetic modes with orbital angular momentum,” *Nature Communications* **9** (2018), 10.1038/s41467-018-07084-2.
- [10] Mengyao Li, Dmitry Zhirihin, Maxim Gorlach, Xiang Ni, Dmitry Filonov, Alexey Slobozhanyuk, Andrea Alù, and Alexander B. Khanikaev, “Higher-order topological states in photonic kagome crystals with long-range interactions,” *Nature Photonics* **14**, 89–94 (2020).
- [11] Aravind Nagulu, Xiang Ni, Ahmed Kord, Mykhailo Tymchenko, Sasank Garikapati, Andrea Alù, and Harish Krishnaswamy, “Chip-scale floquet topological insulators for 5G wireless systems,” *Nature Electronics* **5**, 300–309 (2022).
- [12] Jia Ningyuan, Clai Owens, Ariel Sommer, David Schuster, and Jonathan Simon, “Time- and site-resolved dynamics in a topological circuit,” *Physical Review X* **5**, 021031 (2015).
- [13] Victor V. Albert, Leonid I. Glazman, and Liang Jiang, “Topological properties of linear circuit lattices,” *Physical Review Letters* **114**, 173902 (2015).
- [14] Eric I. Rosenthal, Nicole K. Ehrlich, Mark S. Rudner, Andrew P. Higginbotham, and K. W. Lehnert, “Topological phase transition measured in a dissipative metamaterial,” *Physical Review B* **97**, 220301(R) (2018).
- [15] Marc Serra-Garcia, Roman Süssstrunk, and Sebastian D. Huber, “Observation of quadrupole transitions and edge mode topology in an lc circuit network,” *Physical Review B* **99**, 020304 (2019).
- [16] Nikita A. Olekhno, Egor I. Kretov, Andrei A. Stepanenko, Polina A. Ivanova, Vitaly V. Yaroshenko, Ekaterina M. Puhtina, Dmitry S. Filonov, Barbara Cappello, Ladislau Matekovits, and Maxim A. Gorlach, “Topological edge states of interacting photon pairs emulated in a topoelectrical circuit,” *Nature Communications* **11**, 1436 (2020).
- [17] Zheng Wang, Yidong Chong, J. D. Joannopoulos, and Marin Soljačić, “Observation of unidirectional backscattering-immune topological electromagnetic states,” *Nature* **461**, 772–775 (2009).
- [18] Yihao Yang, Zhen Gao, Haoran Xue, Li Zhang, Mengjia He, Zhaoju Yang, Ranjan Singh, Yidong Chong, Baile Zhang, and Hongsheng Chen, “Realization of a three-dimensional photonic topological insulator,” *Nature* **565**, 622–626 (2019).
- [19] Dmitry V. Zhirihin and Yuri S. Kivshar, “Topological photonics on a small scale,” *Small Science* **1**, 2100065 (2021).
- [20] Juan Song, Fengqing Yang, Zhiwei Guo, Xian Wu, Ke-jia Zhu, Jun Jiang, Yong Sun, Yunhui Li, Haitao Jiang, and Hong Chen, “Wireless power transfer via topological modes in dimer chains,” *Physical Review Applied* **15**, 014009 (2021).
- [21] Li Zhang, Yihao Yang, Zhao Jiang, Qiaolu Chen, Qinghui Yan, Zhouyi Wu, Baile Zhang, Jiangtao Huangfu, and Hongsheng Chen, “Demonstration of topological wireless power transfer,” *Science Bulletin* **66**, 974–980 (2021).
- [22] Farzad Zangeneh-Nejad and Romain Fleury, “Topological analog signal processing,” *Nature Communications* **10**, 2058 (2019).
- [23] Farzad Zangeneh-Nejad and Romain Fleury, “Disorder-induced signal filtering with topological metamaterials,” *Advanced Materials* **32**, 2001034 (2020).
- [24] Andrew Webb, Alena Shchelokova, Alexey Slobozhanyuk, Irena Zivkovic, and Rita Schmidt, “Novel materials in magnetic resonance imaging: high permittivity ceramics, metamaterials, metasurfaces and artificial dielectrics,” *Magnetic Resonance Materials in Physics, Biology and Medicine* (2022), 10.1007/s10334-022-01007-5.
- [25] Alena Shchelokova, Viacheslav Ivanov, Anna Mikhailovskaya, Egor Kretov, Ivan Sushkov, Svetlana Serebryakova, Elizaveta Nenasheva, Irina Melchakova, Pavel Belov, Alexey Slobozhanyuk, and Anna Andreychenko, “Ceramic resonators for targeted clinical magnetic resonance imaging of the breast,” *Nature Communications* **11** (2020), 10.1038/s41467-020-17598-3.
- [26] Viktor Puchnin, Georgiy Solomakha, Anton Nikulin, Arthur W. Magill, Anna Andreychenko, and Alena Shchelokova, “Metamaterial inspired wireless coil for clinical breast imaging,” *Journal of Magnetic Resonance* **322**, 106877 (2021).
- [27] Stanislav I. Maslovski, Pekka M. T. Ikonen, Igor Kolmakov, Sergei A. Tretyakov, and Mikko Kaunisto, “Artificial magnetic materials based on the new magnetic particle: Metasolenoid,” *Progress In Electromagnetics Research* **54**, 61–81 (2005).
- [28] W. P. Su, J. R. Schrieffer, and A. J. Heeger, “Solitons in Polyacetylene,” *Physical Review Letters* **42**, 1698–1701

- (1979).
- [29] Alena V. Shchelokova, Cornelis A.T. van den Berg, Dmitry A. Dobrykh, Stanislav B. Glybovski, Mikhail A. Zubkov, Ekaterina A. Brui, Dmitry S. Dmitriev, Alexander V. Kozachenko, Alexander Y. Efimtcev, Andrey V. Sokolov, Vladimir A. Fokin, Irina V. Melchakova, and Pavel A. Belov, “Volumetric wireless coil based on periodically coupled split-loop resonators for clinical wrist imaging,” *Magnetic Resonance in Medicine* **80**, 1726–1737 (2018).
- [30] Ricardo A. Pinto, Masudul Haque, and Sergej Flach, “Edge-localized states in quantum one-dimensional lattices,” *Physical Review A* **79** (2009), 10.1103/physreva.79.052118.
- [31] L. Jylhä, S. Maslovski, and S. Tretyakov, “High-order resonant modes of a metasolenoid,” *Journal of Electromagnetic Waves and Applications* **19**, 1327–1342 (2005).
- [32] Yiming Gao, Opeyemi Ibidapo, Hildegard K. Toth, and Linda Moy, “Delineating extramammary findings at breast MR imaging,” *RadioGraphics* **37**, 10–31 (2017).
- [33] Alexander Poddubny, Andrey Miroshnichenko, Alexey Slobozhanyuk, and Yuri Kivshar, “Topological majorana states in zigzag chains of plasmonic nanoparticles,” *ACS Photonics* **1**, 101–105 (2014).
- [34] Georgiy Kurganov, Dmitry Dobrykh, Ekaterina Puhtina, Ildar Yusupov, Alexey Slobozhanyuk, Yuri S. Kivshar, and Dmitry Zhirihin, “Temperature control of electromagnetic topological edge states,” *Applied Physics Letters* **120**, 233105 (2022).
- [35] Alexander V. Poshakinskiy, Janet Zhong, Yongguan Ke, Nikita A. Olekhno, Chaohong Lee, Yuri S. Kivshar, and Alexander N. Poddubny, “Quantum Hall phases emerging from atom–photon interactions,” *npj Quantum Information* **7**, 34 (2021).
- [36] Nikita A. Olekhno, Alina D. Rozenblit, Valerii I. Kachin, Alexey A. Dmitriev, Oleg I. Burmistrov, Pavel S. Seregin, Dmitry V. Zhirihin, and Maxim A. Gorlach, “Experimental realization of topological corner states in long-range-coupled electrical circuits,” *Physical Review B* **105** (2022), 10.1103/physrevb.105.l081107.
- [37] Yakir Hadad, Jason C. Soric, Alexander B. Khanikaev, and Andrea Alù, “Self-induced topological protection in nonlinear circuit arrays,” *Nature Electronics* **1**, 178–182 (2018).
- [38] N. Lazarides and G. P. Tsironis, “Topological split-ring resonator based metamaterials with \mathcal{PT} symmetry relying on gain and loss,” *Physical Review B* **102**, 064306 (2020).

SUPPLEMENTARY MATERIAL

Application of topological edge states in magnetic resonance imaging

I. COMPARISON OF EIGENMODES OF STANDARD AND TOPOLOGICAL METASOLENOIDS

To compare the magnetic field distribution of the standard metasolenoid with 7 SRRs and a topological metasolenoid (with dimerization in SRR spacings), we perform a numerical study using Eigenmode Solver in CST Microwave Studio 2021. Both metasolenoids have the same geometric dimensions and considered without any phantoms inside. We compare the magnetic field distributions for the first 5 eigenmodes. The results presented in Fig. S1 show that modes №1,2,3, and 5 have a weak difference in the magnetic field distribution, Fig. S1. At the same time, mode №4 for the topological metasolenoid has a strongly asymmetric magnetic field distribution localized near the edge ring characteristic of a topologically protected edge state, Fig. S1(i).

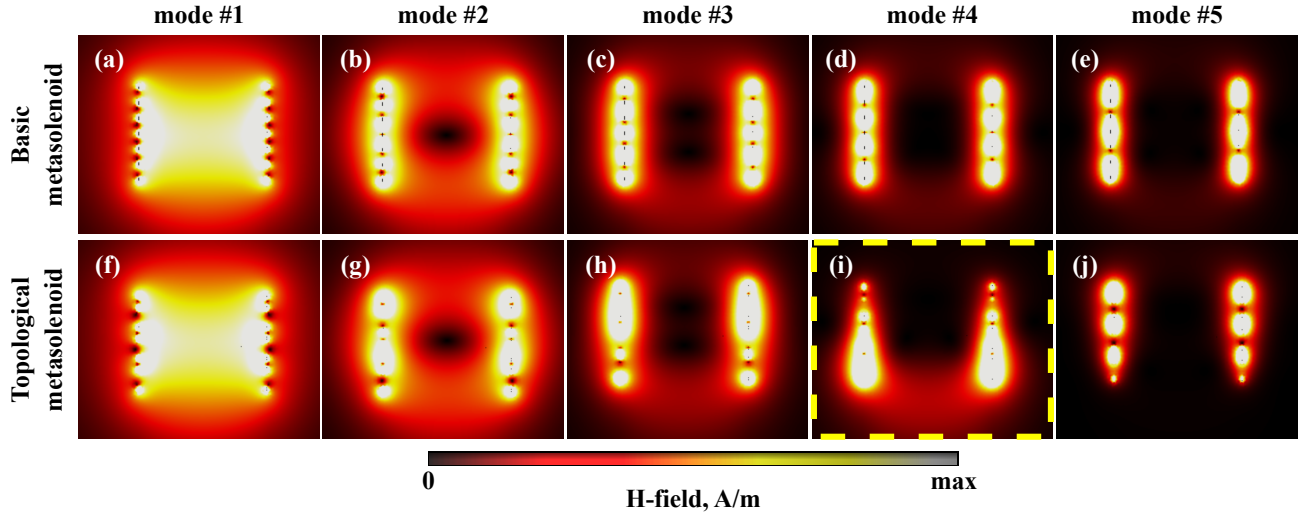


FIG. S1. Numerically calculated H -field distributions of the different eigenmodes for the standard geometry of the metasolenoid (a-e) and for the topological metasolenoid (f-j). The yellow dashed line indicates the topologically protected edge state.

II. EXCITATION OF A TOPOLOGICALLY PROTECTED EDGE STATE USING A STANDARD RF COIL

To investigate the possibility of excitation of a topologically protected edge state in the RF system of a clinical MR scanner, we perform numerical studies using a 16-leg shielded high-pass quadrature whole-body birdcage coil with the inner diameter of 70 cm and the length of 65 cm, tuned and matched to the frequency 63.68 MHz with a homogeneous phantom placed in its center. A circularly polarized RF magnetic field (B_1) is created by two feeding ports with 90° phase shift. The phantom is the same as described in the main text (the size of the body area is $160 \times 160 \times 80 \text{ mm}^3$, the dielectric constant of the body is $\varepsilon = 78$, the conductivity is $\sigma = 0.45 \text{ S/m}$; breast phantom size: the radius is 4.7 cm, the height is 10.34 cm, the dielectric constant is $\varepsilon = 70$, and the conductivity is $\sigma = 0.2 \text{ S/m}$).

We compare two cases: with and without the topological metasolenoid placed around the breast phantom. The comparison is carried out by calculating the root-mean-square value (RMS) of the B_1^+ -field ($|B_1^+|_{\text{RMS}}$) per 1 W of the total accepted power for each case in the breast area. The results demonstrate that using a standard body RF coil, it is possible to excite a topologically protected edge state in the metasolenoid. Such a resonator focuses a transverse RF magnetic field B_1^+ at the border of the phantom's body and breast Fig. S2.

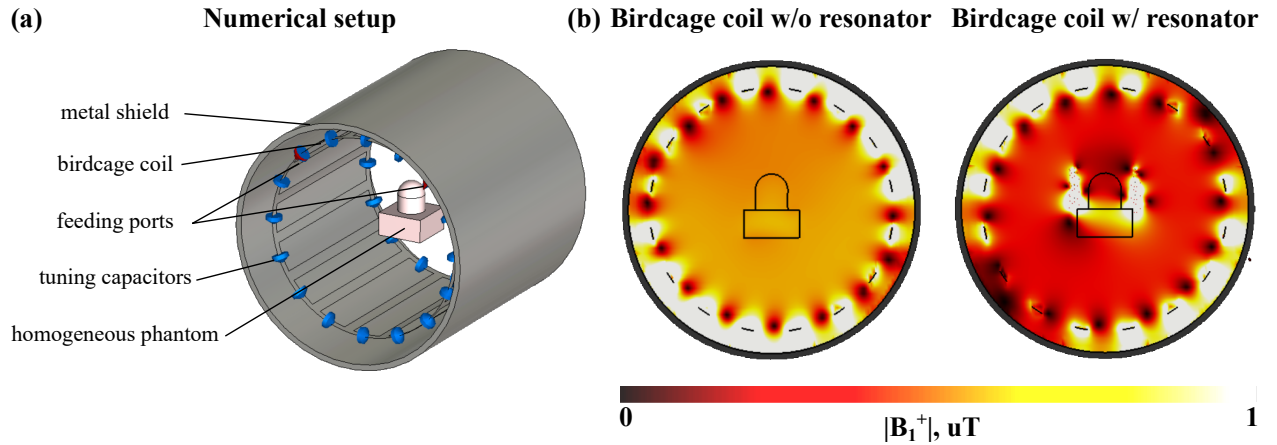


FIG. S2. (a) View of the numerical model which includes a homogeneous phantom placed inside the whole-body birdcage coil model. (b) Numerically calculated $|B_1^+|_{\text{RMS}}$ maps for 1 W of total accepted power without (left) and with (right) the topological metasolenoid.

III. THE REFLECTION SPECTRUM OF A TOPOLOGICAL METASOLENOID.

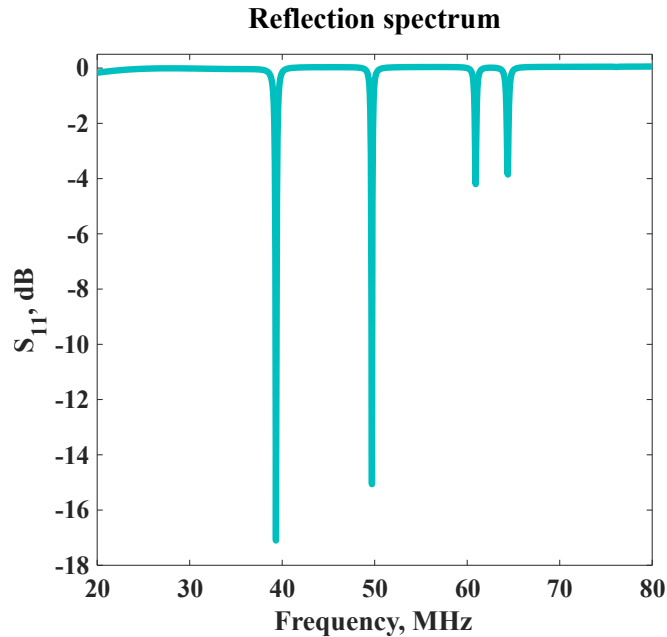


FIG. S3. Experimentally measured reflection spectrum of the topological metasolenoid. The fourth peak corresponds to a topologically protected edge state.

IV. DEPENDENCE OF THE MAGNETIC FIELD AMPLITUDE ON DIMERIZATION

In addition to increasing the SNR, the advantage of using the proposed resonator is the transmit efficiency enhancement. This parameter is defined as the magnitude of the clockwise component of the transverse RF magnetic field (B_1^+) normalized by the accepted power. In other words, an increase in transmit efficiency shows how much it is possible to lower the voltage supplied to the scanner to obtain the same signal level. Less input voltage (or power level) also leads to an improvement of the specific absorption rate (SAR), which is a critical factor in estimating the RF safety of the MR procedure. Therefore, we conduct a numerical study of the dependence of the B_1^+ field amplitude on dimerization. The amplitude was calculated in the part of the phantom mimicking the body. As a result, it is

seen that lower dimerization ratio values correspond to higher transmit efficiency. The obtained maps [Figs.S4(b)-(e)] demonstrate that with increasing dimerization ratio, the localization of the magnetic field B_1^+ near the edge element decreases.

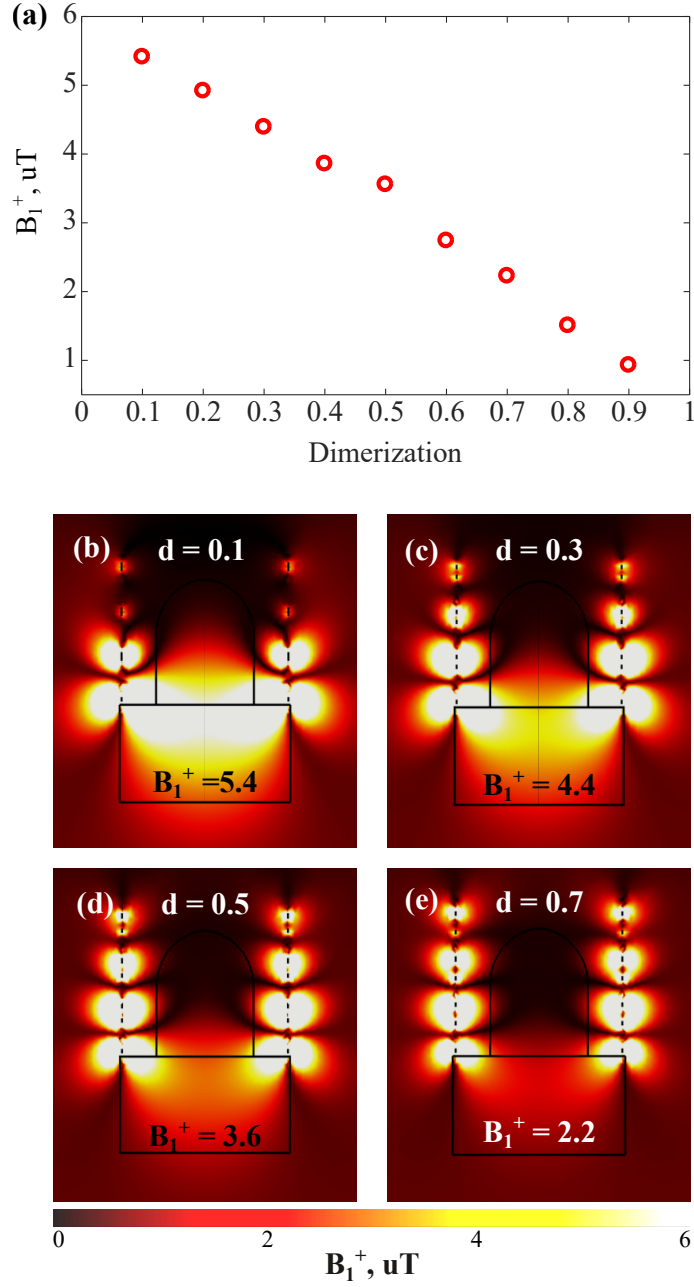


FIG. S4. (a) Numerically obtained B_1^+ amplitude dependence on the dimerization degree. (b-r) B_1^+ distributions for different dimerization degrees d : (b) $d = 0.1$, (c) $d = 0.3$, (d) $d = 0.5$, and (e) $d = 0.7$.